Fabrication of Size-Tunable Gold Nanoparticles Array with Nanosphere Lithography, Reactive Ion Etching, and Thermal Annealing

B. J. Y. Tan,[†] C. H. Sow,*[,†,‡] T. S. Koh,[†] K. C. Chin,[‡] A. T. S. Wee,[†,‡] and C. K. Ong[†]

Department of Physics, Blk S12, Faculty of Science, National University of Singapore, 2 Science Drive 3, Singapore 117542, and National University of Singapore Nanoscience and Nanotechnology Initiative, 2 Science Drive 3, Singapore 117542

Received: October 22, 2004; In Final Form: April 8, 2005

Two-dimensional ordered arrays of gold (Au) nanoparticles were fabricated using two different variants of the nanosphere lithography technique. First, ordered arrays of polystyrene nanospheres on Si substrate were used as deposition masks through which gold films were deposited by electron beam evaporation. After the removal of the nanospheres, an array of triangular Au nanodisks was left on the Si substrate. After thermal annealing at increasing temperature, systematic shape transition of the nanostructures from original triangular Au nanodisks to rounded nanoparticles was observed. This approach allows us to systematically vary the size and morphology of the particles. In the second and novel technique, we made use of reactive ion etching to simultaneously reduce the dimension of the masking nanospheres and create arrays of nanopores on the substrate prior to the deposition of the Au films. These samples were subsequently annealed, which resulted in size-tunable and ordered Au nanoparticle arrays with the nanoparticles nested in the nanopores of the templated substrate. With the nanoparticles anchored in the nanopores, the substrate could be useful as a template for growth of other nanomaterials.

Introduction

The fabrication of periodic arrays of nanoparticles has been a subject of great interest because of their size-dependent properties. These nanoparticles have found potential applications as biosensors,[1−5] chemical sensors, optical devices,[6−9] magnetic data storage memory bits,[10] templates for the growth of other nanomaterials,[11−13] etc. The nanoparticles are also useful in the study of coherent phonon oscillation.[14] A variety of techniques have been developed to fabricate ordered arrays of nanoparticles. Among these techniques, electron beam lithography and focused ion beam lithography are able to fabricate arrays of nanoparticles with excellent size, shape, and spacing control. However, the cost of these techniques is rather high and the process of fabrication could be slow because of their serial nature. Many researchers have focused on the development of alternative parallel lithographic methods. Among these techniques, nanosphere lithography (NSL) is a versatile, high-throughput, low-cost and parallel technique that is frequently utilized in the fabrication and studies of nanoparticle arrays.[15−17] In NSL, ordered arrays of polystyrene nanospheres on Si substrates are used as deposition masks through which a thin film of the desired materials is deposited. After the removal of the nanospheres, an array of nanoparticles in the shape of triangular nanodisks is left on the Si substrate. One can readily control the size of the nanoparticles by using different sized nanospheres as deposition masks. In addition, combining NSL with thermal annealing, one can transform the shape of the nanoparticles from a typical triangular disk to that of rounded nanoparticles.[18−20] On the other hand, by means of reactive ion etching (RIE), one can reduce the dimension of the nanospheres without changing the center-to-center distance of the nanospheres.[21−24] With this added process, it is possible to extend the technique of NSL from the creation of nanoparticle arrays to the fabrication of continuous networks of materials.[25]

In this work, we present our efforts on further development of two different variants of the NSL technique. Henceforth, we shall refer to these two techniques as $NSL_{annealing}$ and $NSL_{RIE-annealing}$ techniques. In the $NSL_{annealing}$ technique, similar to earlier reports by other researchers,[18−20] we made use of NSL with thermal annealing in the fabrication of a gold (Au) nanoparticle array. However, in contrast to previous reports, we have studied the systematic transformation of the nanoparticles by investigating the shape of the nanoparticles after thermal annealing at increasing temperatures. The range of annealing temperatures investigated was from 205 to 930 °C. In this way, the systematic shape transformation of the Au nanoparticles from the original triangular Au nanodisks to rounded nanoparticles was observed.

The $NSL_{RIE-annealing}$ technique is a variant of the $NSL_{annealing}$ technique with an additional step of reducing the size of the masking nanospheres via RIE before thermal evaporation of a gold film. In this way, periodic arrays consisting of Au particles of increasing size or a continuous network of Au could be fabricated depending on the duration of the RIE process. These samples were subsequently annealed in stages at increasing temperatures. During the RIE process, the Si substrate was patterned with a periodic array of nanopores.[26] These nanopores served as holding cages for the resultant nanoparticles during the annealing process. After annealing, the Au nanoparticles were found nested in the nanopores of the templated substrate. With the annealed nanoparticles caged in the nanopores, the substrate with patterned nanoparticles could serve as a useful template for deposition or growth of other materials with minimum movement of the nanoparticles during any postprocessing treatments.

* Corresponding author. Phone: (65) 68742957. Fax: (65) 67776126. E-mail: physowch@nus.edu.sg.

[†] National University of Singapore.

[‡] National University of Singapore Nanoscience and Nanotechnology Initiative.

10.1021/jp045172n CCC: $30.25
Published on Web 05/13/2005

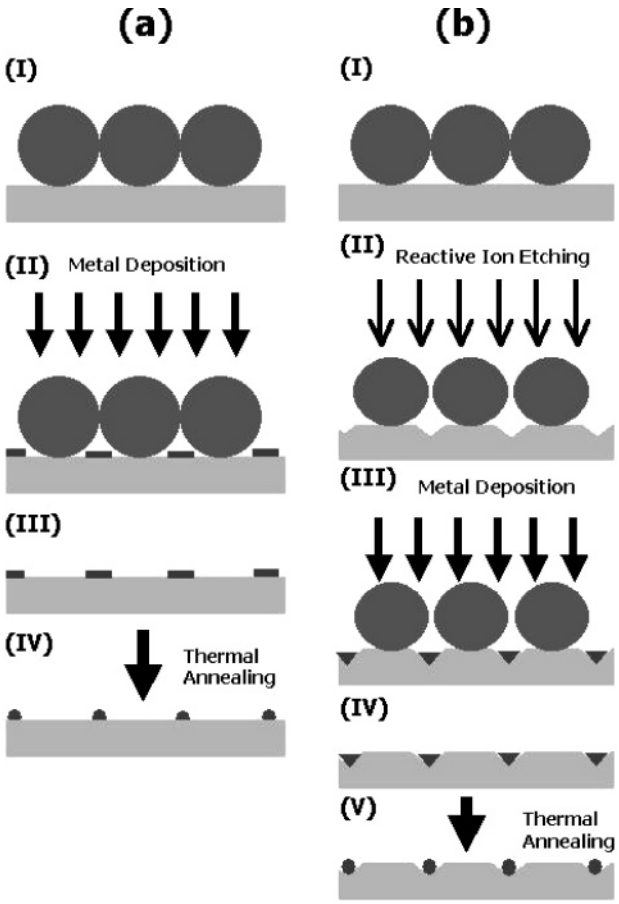

Figure 1. Schematics of the two fabrication processes.

Experimental Section

The two nanofabrication techniques employed in this work are illustrated in Figure 1. Figure 1a summarizes the conventional $NSL_{annealing}$ process. The nanoparticles were patterned on Si substrates that were cut from n-type Si(100) wafers of about 10×10 mm^2. The substrates were first cleaned in a solution consisting of 4 parts sulfuric acid (H_2SO_4, 12 M) to 1 part hydrogen peroxide (H_2O_2, 20% solution) and then thoroughly rinsed with boiling, deionized water. The nanosphere lithography masks were formed using polystyrene spheres (Polysciences) with diameters of 356 and 1053 nm. The nanospheres were either spin-coated (at 950 rpm) onto the substrate or coated by way of convective deposition. The nanospheres self-assembled into a hexagonal close-packed array suitable for use as a lithographic mask. After the formation of the nanosphere mask on the substrates, gold was deposited onto the masked substrates by vaporizing pure Au targets in a Leybold Univex 300 electron beam evaporator system at a base pressure of around 5×10^{-6} Torr. The thicknesses of the coated films were measured by an oscillating quartz plate placed at the same distance from the source as the sample (~18 cm). Following the deposition, the nanosphere masks were removed by dissolution in dicholoromethane (CH_2Cl_2) with the aid of sonication. In all of the annealing processes, a tube furnace was first heated to the target temperature before the sample was loaded into the furnace. The temperature of the furnace was kept within $\pm 5-7$ °C of the target temperature during the annealing. The range of annealing temperatures investigated was between 205 and 930 °C, and the annealing was carried out in ambient. After the sample was annealed for 30 min, the heater was turned off and the sample was left to cool in the furnace to room temperature. In addition, a sample was heated using a hot plate maintained at about 350 °C. Before and after the annealing, the samples were studied using scanning electron microscopy (SEM; JEOL JSM-6400F field emission scanning electron microscope and Philips Model FEG XL-30 scanning electron microscope).

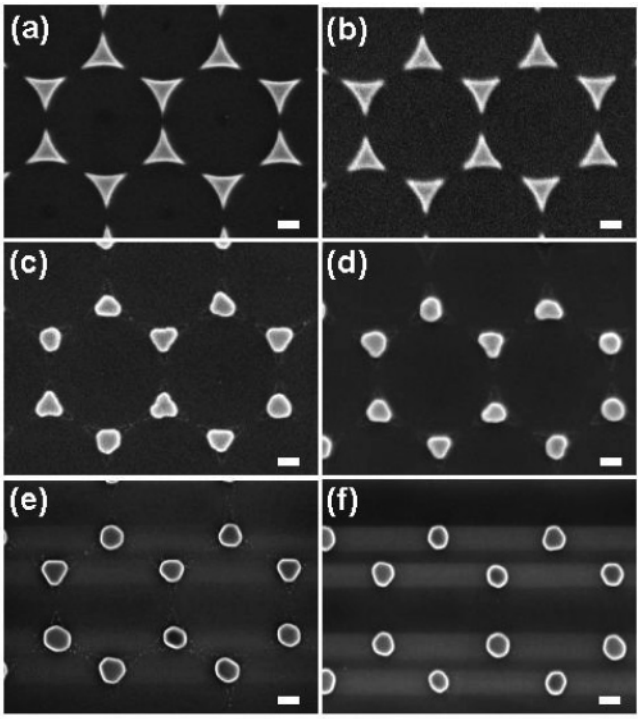

Figure 2. SEM images of (a) as-deposited and (b−f) annealed Au nanoparticles. The sample was annealed in stages with increasing temperatures at each stage, and the images were obtained after each annealing step. The corresponding annealing temperatures were (b) 205, (c) 325, (d) 451, (e) 700, and (f) 930 °C. Scale bars = 200 nm.

The $NSL_{RIE-annealing}$ process as illustrated in Figure 1b is similar to the $NSL_{annealing}$ process but with an additional step of sample treatment. Before the deposition of the Au film, the nanosphere masked substrates were placed inside the chamber of a SAMCO RIE-10N reactive ion etching unit and pumped down to a base pressure of 4×10^{-6} Torr. An rf glow discharge was used to generate the reactive ions. The samples were placed on an rf-driven capacitatively coupled electrode. A gas mixture of tetrafluoromethane (CF_4) at 29.7 sccm and oxygen (O_2) at 17.3 sccm was utilized during the etching. The forward rf power was 20 W, and reflected power was 1− 2 W. The duration of the etching was varied from 4 to 12 min. In this way, the diameters of the masking nanospheres were systematically reduced prior to the deposition of Au. As a result, arrays consisting of Au particles of increasing size were created. With longer etching time, the deposited Au joined together to form a continuous network of nanoholes. These samples were then annealed, and again the systematic transformation of the structured Au film was studied.

Results and Discussion

Size of Nanoparticles versus Annealing Temperature. $NSL_{annealing}$ was first carried out using polystyrene nanospheres of uniform size and with a diameter of 1053 nm. Fifty nanometers of Au was deposited onto the masked substrate at a rate of 1 Å/s. After the removal of the polystyrene nanospheres, an array of Au nanoparticles in the form of triangular nanodisks was left behind on the substrate (Figure 2a). The sample was first annealed in a tube furnace at 205 °C (Figure 2b) in ambient for 30 min followed by SEM imaging. The shape

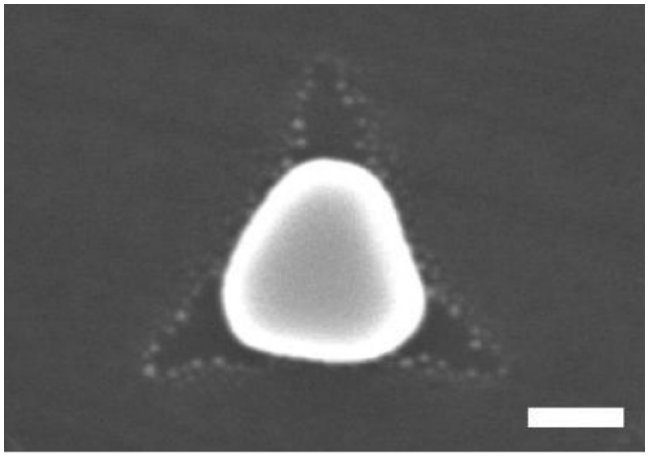

Figure 3. SEM image of a close-up view of an annealed nanoparticle. The profile of the triangular nanodisks prior to annealing is clearly visible. Scale bar = 100 nm.

of the Au nanoparticles remained unchanged. The sample was then annealed at 325 °C for 30 min and imaged again. As can be seen in Figure 2c, the Au forming the apexes of triangular nanodisks has started to retract, resulting in triangular Au nuggets. Further annealing at 451 °C for 30 min resulted in the appearance of more rounded Au nanoparticles and faceting dots (Figure 2d). Thermal annealing was further carried out at 700 °C (Figure 2e) and 930 °C (Figure 2f) for 30 min each, after which we found more rounded nanoparticles and faceting dots with further reduction in the dimensions of the particles. It should be noted that, in similar experiments carried out by other researchers,[18−20] annealing of the as-deposited triangular nanodisks at high temperature resulted in more rounded nanoparticles. In our approach, annealing the as-deposited nanodisks at different and intermediate temperatures provides an added control in fabricating nanoparticles with a shape that is between the two extremes. In this work, the bulk of the thermal annealing was carried out using the tube furnace. However, we have also carried out similar experiments where samples decorated with Au triangular nanodisks were annealed with a hot plate maintained at a constant temperature of 350 °C in ambient. In this case, the shape of the annealed nanoparticles was found to be similar to those shown in Figure 2c,d.

Figure 3 shows a close-up SEM image of an annealed Au nanoparticle after thermal annealing at 350 °C. The profile of the triangular nanodisks before thermal annealing is clearly visible in the figure. The facets of the nanoparticle correspond to the apexes of the triangular nanodisks prior to thermal annealing. We have employed an annealing temperature that is lower than the melting point of bulk gold (1063 °C). However, the annealing temperatures were sufficiently high to cause surface melting of the Au material at the apexes of the triangular nanodisks. As a result, the surface tension of the melted Au material caused the "retraction" of these softened apexes, forming the observed more rounded shape. It should be noted that, for nanoscale materials, their melting point is expected to be lower than the melting point of the corresponding bulk material.[27−29] Thus we were able to cause shape transformation of these triangular nanodisks despite the fact that the annealing temperatures employed were comparatively lower than the bulk melting temperature. Hulteen et al.[29] reported that formation of rounded silver nanoparticles that was attributed to surface melting was possible even at room temperature.

Histograms of the size distributions of the Au nanoparticles (as shown in Figure 2) created by the $NSL_{annealing}$ technique are shown in Figure 4. In the case of triangular nanodisks, the size

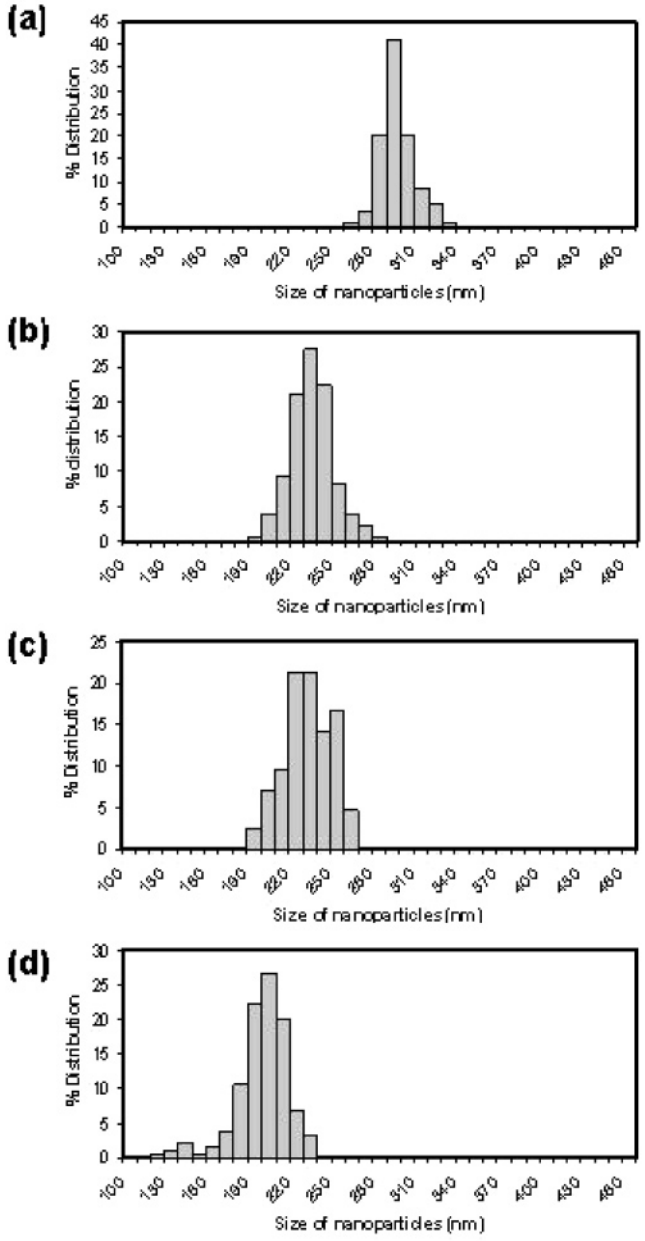

Figure 4. Histograms of size distributions of (a) as-deposited Au nanoparticles and after annealing at (b) 325, (c) 451, and (d) 930 °C.

of the nanoparticle refers to the length from an apex of the triangle to its base. The average size of the as-deposited Au nanoparticles was about 287 nm (Figure 4a). After thermal annealing at 325 °C (Figure 4b), 451 °C (Figure 4c), and 930 °C (Figure 4d), the average size of the nanoparticles was reduced to 226, 223, and 190 nm, respectively. In addition, the standard deviation of the size distribution of the nanoparticle was found to increase slightly. The measured values were (a) 12, (b) 16, (c) 19, and (d) 19 nm.

The height and volume of the nanoparticles were determined with an atomic force microscope (AFM) (DI Dimension 3100 NanoMan) at each stage of the thermal annealing. From the line section of the profile of the particle, we found that the average maximum height of the nanoparticles increased as they were annealed. In addition, AFM analysis also facilitated the computation of the volume of the nanoparticles. Figure 5 shows a plot of the measured average volume of the nanoparticles after each stage of thermal annealing. The average volume of the nanoparticles was found to increase from room temperature to

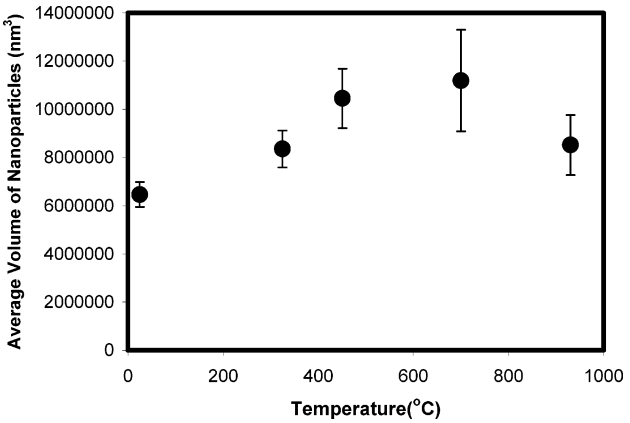

Figure 5. Graph of average volume of annealed nanoparticles versus annealing temperature.

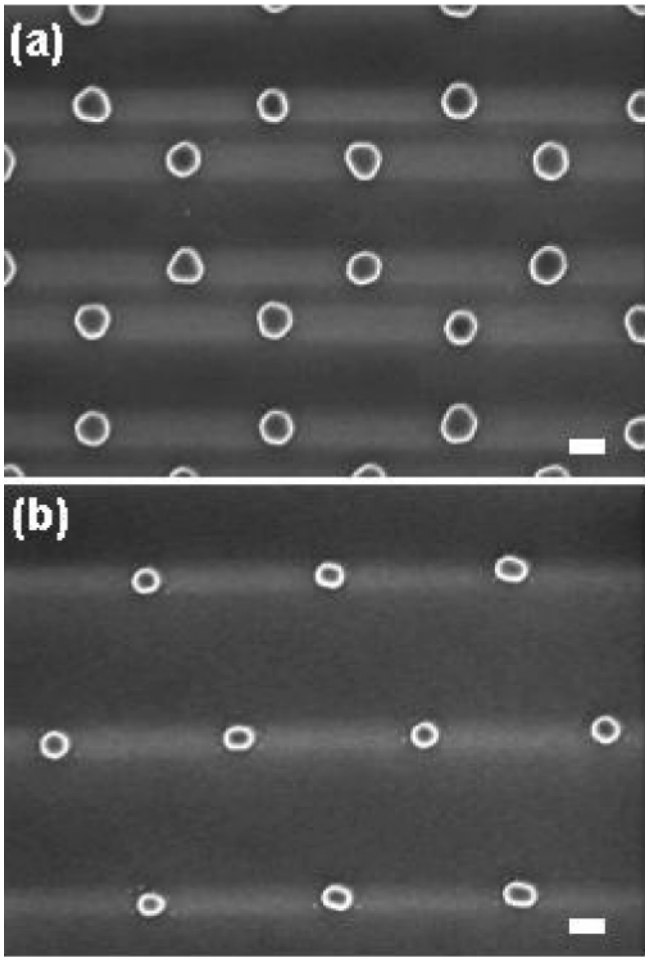

Figure 6. SEM images of annealed (final annealing temperature of 930 °C) Au nanoparticles arrays found in region previously covered with (a) a monolayer of nanospheres and (b) double layers of nanospheres. Scale bars = 200 nm.

700 °C. After the particle was annealed to 930 °C, the average volume of the nanoparticles decreased. The increase in the average volume of the nanoparticles could be attributed to the formation of oxide/silicide[30,31] materials during the annealing process since the heating of the nanoparticles on the silicon substrate was carried out in ambient. The decrease in volume at 930 °C is probably due to the high annealing temperature that caused material evaporation.

In NSL, it is common to make use of double-layered masks to fabricate periodic arrays of nanoparticles with increased

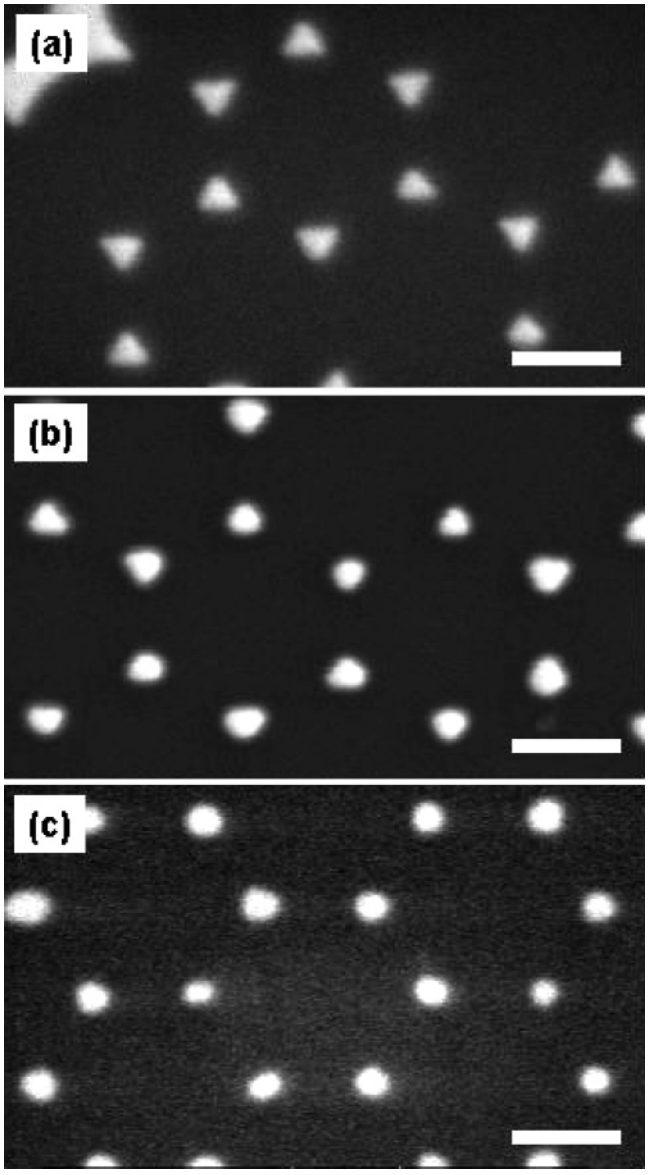

Figure 7. SEM images of (a) as-deposited and annealed Au nanoparticles at (b) 351 and (c) 500 °C. The diameter of the nanospheres employed in the $NSL_{annealing}$ process was 356 nm. Scale bars = 200 nm.

distances between the particles. A similar approach could be adopted in the $NSL_{annealing}$ technique. SEM images of an annealed Au nanoparticle array found at regions of the substrate that were previously covered with (a) a monolayer and (b) double layers of nanospheres can be seen in Figure 6. Again the sample was annealed in stages and the final annealing temperature was 930 °C. The thickness of the Au film deposited was 50 nm. The average size of the particles is in (a) 211 ± 12 nm and in (b) 162 ± 12 nm. The size ratio of 0.76 is consistent with the ratio of 0.7−0.8 obtained in normal NSL.[32]

Effect of Different Size Nanospheres. In NSL, one can readily control the size of the nanoparticles using ordered arrays of nanospheres of different diameters as a mask. Extending this approach to $NSL_{annealing}$, SEM images of arrays of (a) as-deposited and (b,c) annealed Au nanoparticles are illustrated in Figure 7. In these cases, the diameter of the nanospheres used was 356 nm and the thickness of the Au film deposited was 30 nm. The annealing temperatures employed were (b) 351 and (c) 500 °C. The average dimension of the annealed nanoparticles was about (a) 64 ± 5, (b) 59 ± 6, and (c) 55 ± 6 nm. Naturally,

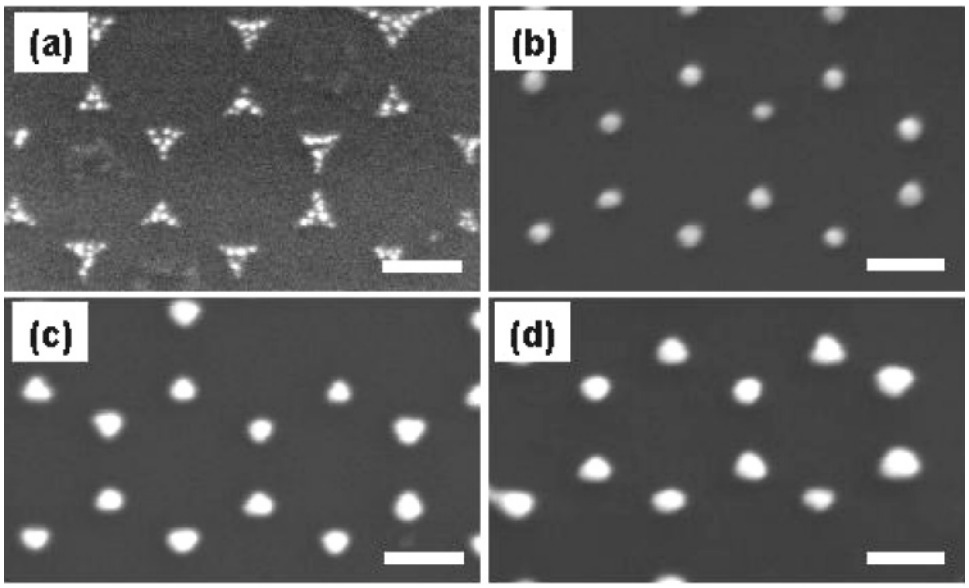

Figure 8. SEM images of Au nanoparticles arrays fabricated by $NSL_{annealing}$ at 351 °C. The diameter of the polystyrene nanospheres used was 356 nm, and the thicknesses of the Au deposited prior to thermal annealing were (a) 2, (b) 10, (c) 30, and (d) 100 nm. Scale bars = 200 nm.

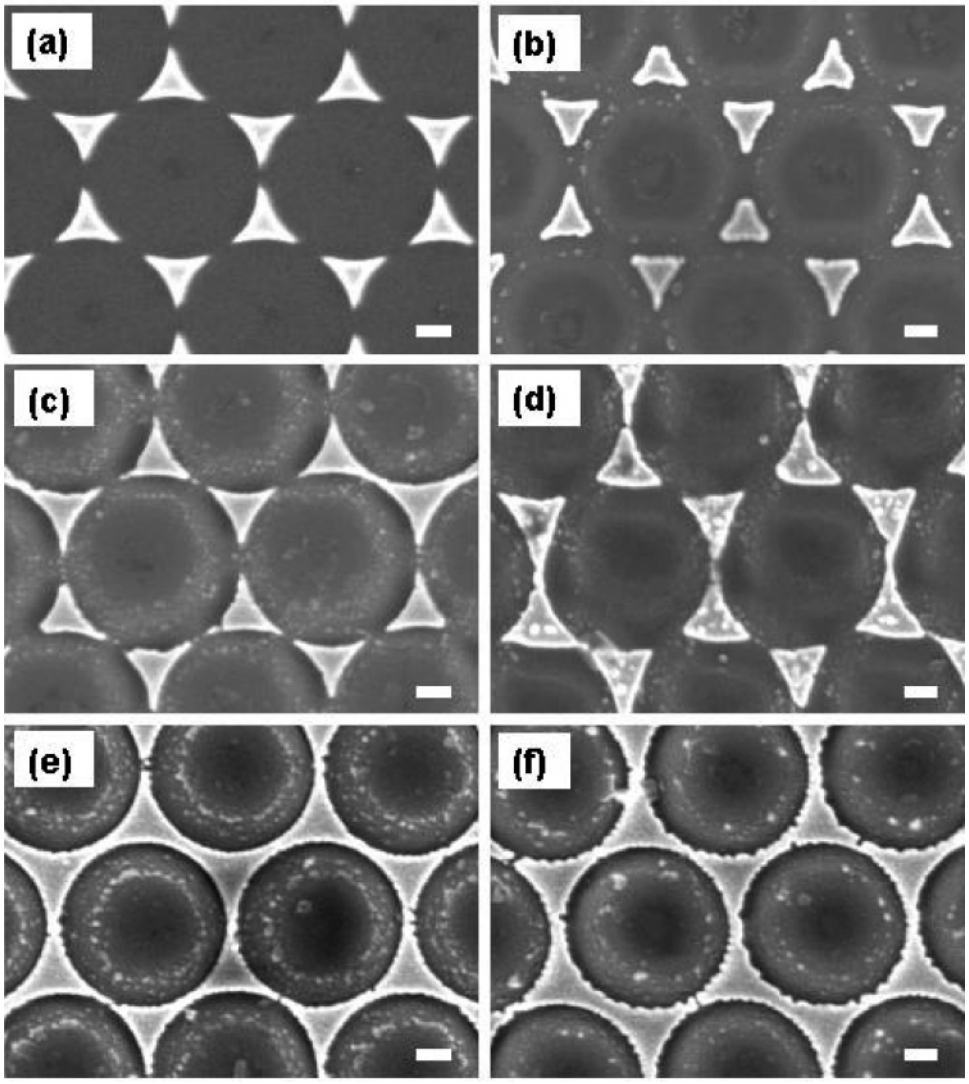

Figure 9. SEM images of (a) Au nanoparticles array formed on Si substrate without etching of the nanospheres mask, and (b−f) Au structures formed after etching the nanospheres mask with RIE. The duration of the etching was (b) 4, (c) 6, (d) 8, (e) 10, and (f) 12 min. Scale bars = 200 nm.

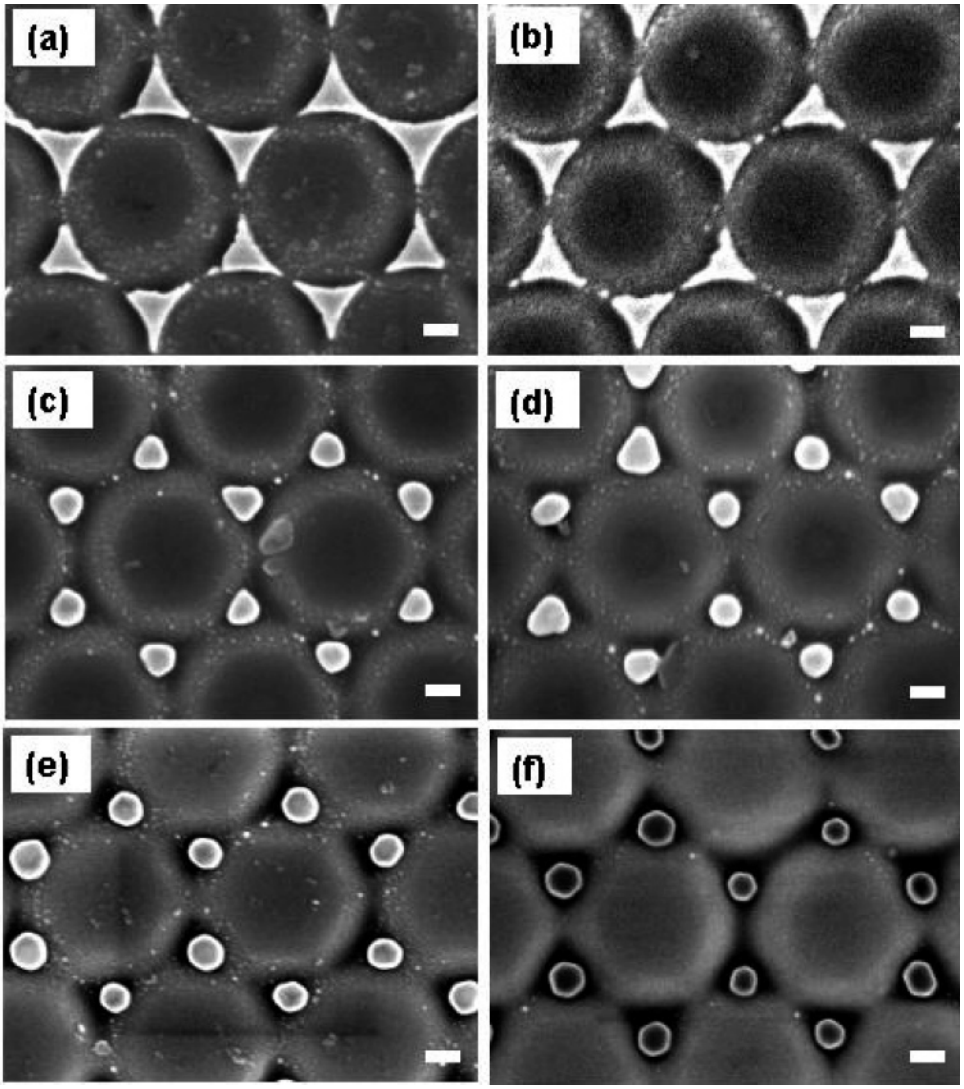

Figure 10. SEM images of (a) as-deposited and (b−f) annealed Au nanoparticles. The masked substrate was exposed to 6 min of RIE prior to Au deposition. The sample was annealed in stages with increasing temperatures, and the images were obtained after each annealing steps. The corresponding annealing temperatures were (b) 205, (c) 325, (d) 451, (e) 700, and (f) 930 °C. Scale bars = 200 nm.

with smaller nanospheres as a mask, the dimension of the nanoparticles created would be smaller. Furthermore, the shape transformation from triangular nanodisks into rounded nanoparticles could be achieved at a lower annealing temperature. This is due to the larger surface area to volume ratio for the smaller nanoparticles.

Effect of Different Deposited Au Thickness. In this work, we have also investigated the effect of different deposited Au thicknesses on the size and shape of the annealed nanoparticles. Figure 8 shows SEM images of nanoparticles on Si fabricated by $NSL_{annealing}$ at 351 °C. The diameter of the nanospheres used was 356 nm. The thicknesses of the Au film deposited were (a) 2, (b) 10, (c) 30, and (d) 100 nm, respectively. Figure 8a shows that, for a thin layer of Au film, the triangular nanodisks became disintegrated and comprised of disjointed nanoparticles with random sizes scattered throughout the original triangular area. Li et al.[19] reported similar observations for Ge nanoparticles. With thicker layers of Au deposited, parts b−d of Figure 8 show the systematic increment in dimension of the annealed nanoparticles with increasing thickness of the deposited Au film. These images demonstrate the feasibility of fabrication of size-tunable annealed Au nanoparticles with different thicknesses of the Au deposited. From our measurements, the dimension of the nanoparticles in Figure 8b is 59.4 ± 5.9 nm and the dimension of the nanoparticles in Figure 8d is 78.5 ± 11.0 nm.

NSL−Thermal Annealing with Reactive Ion Etching. $NSL_{RIE-annealing}$ technique is useful in fabricating a size-tunable nanoparticle array with the nanoparticles caged in periodic pockets (nanopores) etched onto the Si substrate. When an ordered array of polystyrene nanospheres was exposed to reactive ion plasma from a gas mixture of CF_4 and O_2 in a reactive ion etching (RIE) system, the active ions etched and reduced the size of the nanospheres without disturbing the periodic spacing of the nanospheres.[21−24] Simultaneously, the reactive ions created periodic arrays of etched pockets on the Si substrate. As a result of the reduction in the size of the masking nanospheres, the size of the vacancies through which material deposited onto the substrate during NSL increases. Thus by reactive ion etching of the nanospheres and substrate prior to the Au deposition, arrays consisting of nanoparticles of increasing size (without changing the lattice spacing of the particles) were fabricated. With longer etching time, the area covered by the deposited Au increases and they eventually merge together to form a continuous network of Au nanoholes.

The systematic transformation of the as-deposited Au from nanoparticles to nanoholes is shown in Figure 9. The diameter

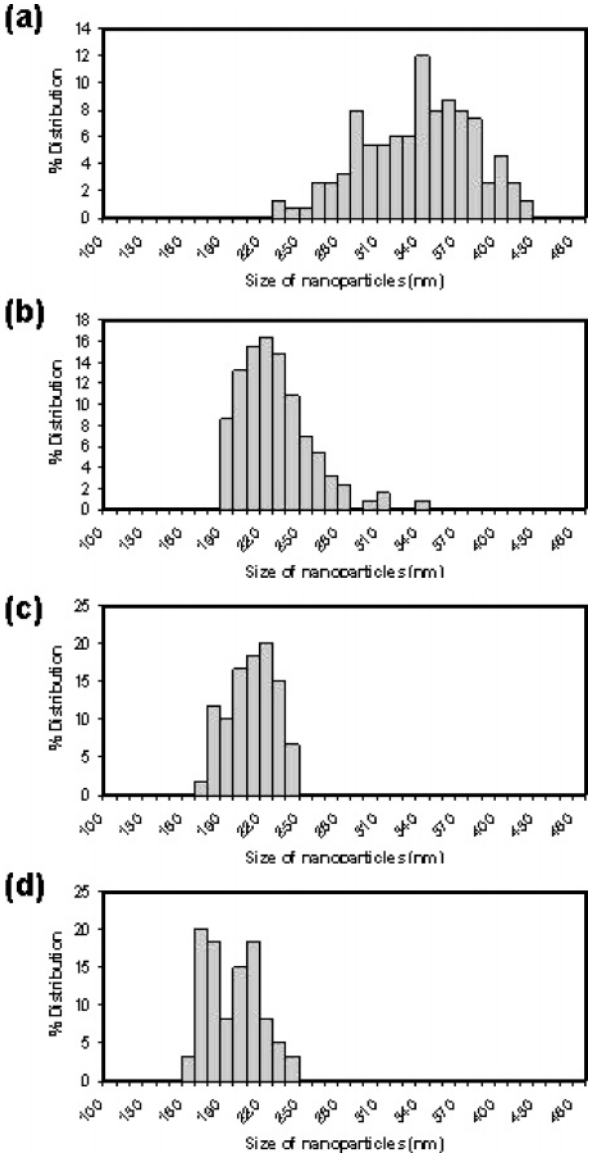

Figure 11. Histograms of size distributions of (a) as-deposited Au nanoparticles and after annealing at (b) 451, (c) 700, and (d) 930 °C. In this case, the masked substrate was exposed to 6 min of RIE prior to Au deposition and thermal annealing.

of the spheres used was 1053 nm, and the duration of the exposure to reactive ion etching ranged from 4 to 12 min. In these cases, the thickness of the Au film deposited was 50 nm. A similar approach was adopted by Murray et al. in the creation of arrays of silver nanoparticles and nanoholes.[25] It is interesting to note that Figure 9a,b shows a slight reduction in the dimension of the deposited Au triangular nanodisks. This could be due to the fact that the Au film was deposited onto a contoured substrate in Figure 9b instead of the flat substrate in Figure 9a.

The added process of RIE in NSL with annealing facilitates additional control over the size of the particles. In addition, the substrate with etched pattern presents ideal housing pockets in which the annealed nanoparticles reside. After the deposition of the Au nanoparticles, the nanospheres were removed and the sample was again annealed at different stages with increasing temperatures. The shape transformation of the nanoparticles in one such sample is indicated in Figure 10. The masked sample was exposed to reactive ion etching for 6 min prior to deposition of 50 nm of Au and annealing. The RIE process created patterned Si substrates with periodic pockets, and they became natural pockets that house the annealed nanoparticles. The

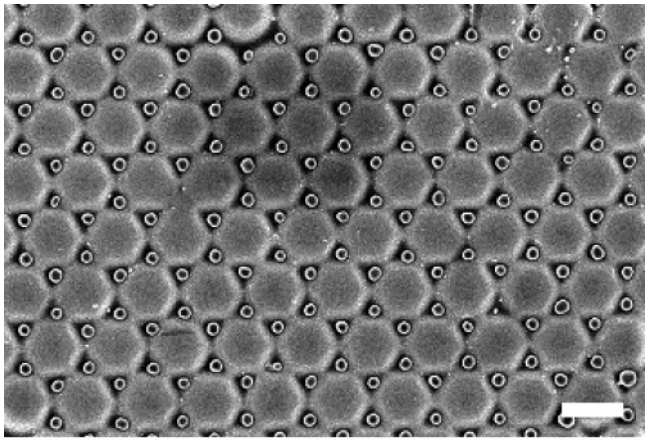

Figure 12. SEM image of a patterned substrate with one-to-one correspondence between the annealed nanoparticles and the nanopores. Scale bar = 1 μm.

etching rate of the masked Si substrate was about 20 nm/min, so with 6 min of exposure to reactive ions, the maximum depth of the pockets was about 120 nm.

Histograms of the size distributions of the Au nanoparticles (as shown in Figure 10) created by the $NSL_{RIE-annealing}$ technique are illustrated in Figure 11. In this case, the masked substrate was exposed to 6 min of RIE prior to Au deposition and thermal annealing. It can be noted that the average size of the as-deposited Au nanoparticles was about 336 nm (Figure 11a). It has a rather broad distribution compared to the one shown in Figure 4a. The standard deviation of the particle size distribution was found to be about 50 nm. This broad distribution could be due to the greater size variation of the masking polystyrene particles after the process of RIE. After thermal annealing at 451 °C (Figure 11b), 700 °C (Figure 11c), and 930 °C (Figure 11d), the average size of the nanoparticles was reduced to 222, 204, and 189 nm, respectively. In addition, the standard deviation of the size distribution of the nanoparticles was found to reduce significantly. The measured values were (b) 27, (c) 18, and (d) 21 nm, respectively. Hence thermal annealing in this case helps to reduce the average size of the particles and narrow its size distributions.

One of the active areas of research in nanopatterning is the use of a patterned template for the directed assembly of other micro- or nanoparticles.[33−36] In these experiments, typically an aqueous suspension of nanoparticles is required and the nanoparticles are deposited onto the template via controlled drying. A variety of configurations can be obtained in this way depending on the concentrations of the particles, drying rate, etc. One of the advantages of our technique is that it is straightforward to achieve one-to-one correspondence between the annealed nanoparticles and the nanopores. In Figure 12, an SEM image of a patterned substrate with one-to-one correspondence between the annealed nanoparticles and the nanopores is shown. The masked substrate was first exposed to RIE for 6 min, followed by deposition of 50 nm of Au. The SEM image shown was obtained after thermal annealing at 700 °C. With the annealed nanoparticles caged in the added holding pockets, the substrate could potentially be useful as a template for growth of other materials whereby Au nanoparticles could serve as a catalyst (e.g., for the growth of ZnO nanowires[12,37,38]). It could also possibly withstand more adverse processing treatment with the nanoparticles anchored in their intended location.

The shape transformation of the nanoholes array in this combined NSL−RIE−thermal annealing process is shown in Figure 13. The masked substrate was first exposed to RIE for

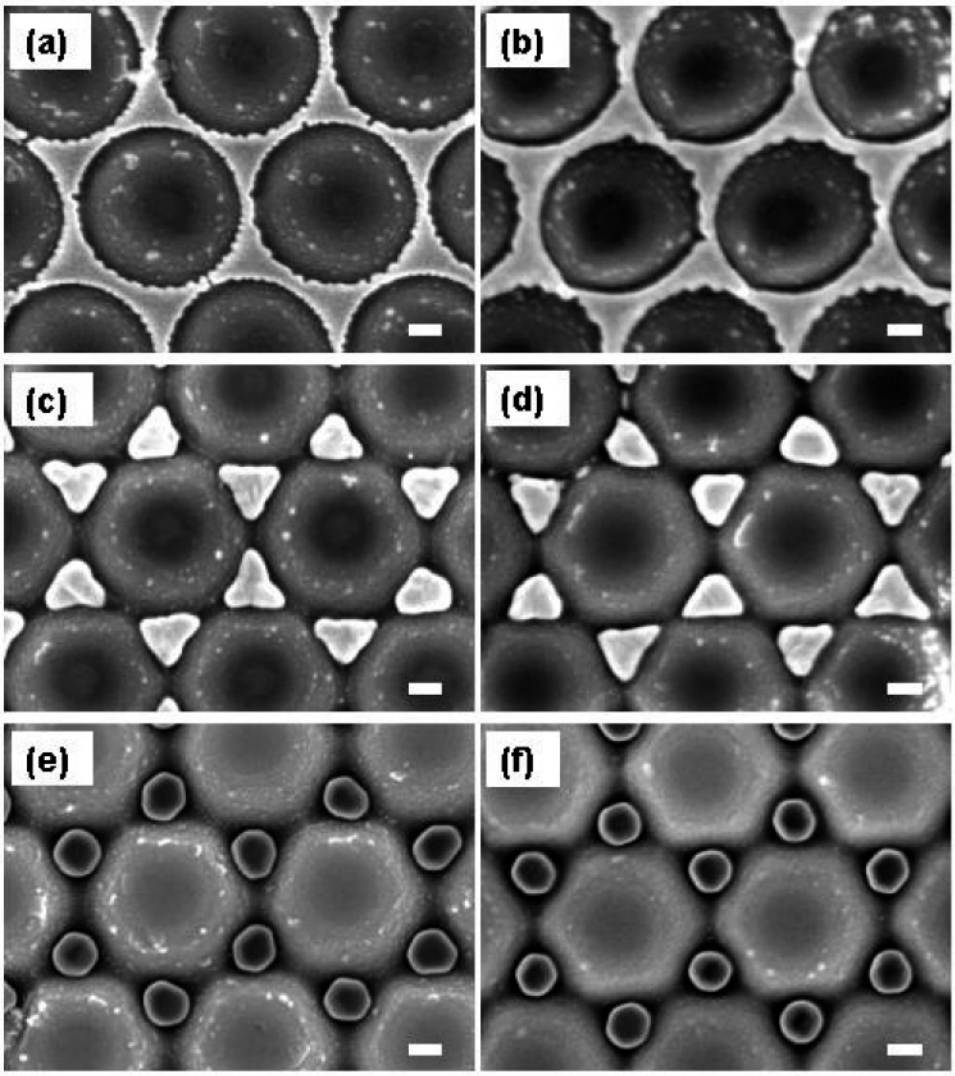

Figure 13. SEM images of (a) as-deposited and (b−f) annealed Au nanoparticles. The masked substrate was exposed to 12 min of RIE prior to Au deposition. The sample was annealed in stages with increasing temperatures at each stage, and the images were obtained after each annealing step. The corresponding annealing temperatures were (b) 205, (c) 325, (d) 451, (e) 700, and (f) 930 °C. Scale bars = 200 nm.

12 min prior to the deposition of 50 nm of Au. In this case, we found a continuous network of Au nanoholes as evidenced in Figure 13a. Upon mild thermal annealing at 205 °C (Figure 13b), we did not find significant shape transformation. After further annealing at 325 °C (Figure 13c), the Au network was found to disintegrate into a triangular nanoparticle array. It should be noted that the average size of these triangular nanoparticles was about 64% larger than those shown in Figure 2c even though the size of the nanospheres used, the annealing temperature, and the thickness of the Au film deposited were the same in these two experiments. At higher annealing temperatures (Figure 13d−f), these triangular nanoparticles underwent a further shape transformation into a more rounded shape. Figures 10 and 13 illustrate the feasibility of using reactive ion etching as an added processing step to fabricate and tune the size of the nanoparticles.

The size distributions of the Au nanoparticles (as shown in Figure 13) created by the $NSL_{RIE-annealing}$ technique are plotted in histograms (Figure 14). In this case, the masked substrate was exposed to 12 min of RIE prior to Au deposition and thermal annealing. The histograms correspond to size distribution of the Au nanoparticles formed after thermal annealing at 325 °C (Figure 14a), 451 °C (Figure 14b), 700 °C (Figure 14c), and 930 °C (Figure 14d), respectively. The average sizes of the annealed nanoparticles were found to be (a) 297, (b) 314, (c) 280, and (d) 264 nm, respectively. The corresponding measured standard deviations of the size distribution were (a) 27, (b) 32, (c) 18, and (d) 15 nm. Again thermal annealing at higher temperature produces nanoparticles with narrower size distribution.

For a better view of the side profile of the sample, an oblique view SEM image of the annealed Au nanoparticle array on a patterned (12 min of RIE) substrate is shown in Figure 15. The depth of the etched nanopores can be seen to be larger than the thickness of the annealed Au nanoparticle. As a result, the Au nanoparticles became embedded in the patterned Si substrate. To reveal the embedded Au nanoparticle, we carefully cleaved the Si substrate and mounted it for SEM imaging. Depending on the duration of RIE, the depth of the etched nanopores could be controlled such that the annealed Au nanoparticle become elevated from or embedded in the substrate.

With a double-layered mask in the $NSL_{RIE-annealing}$ technique, we could fabricate periodic particle arrays with larger spacing and smaller particles in nanopores. Figure 16 shows the result of the $NSL_{RIE-annealing}$ technique with the substrate previously covered with double layers of nanospheres. The duration of the RIE employed was 10 min, the thickness of the Au deposited was 50 nm, and the annealing temperature was 350 °C for 30

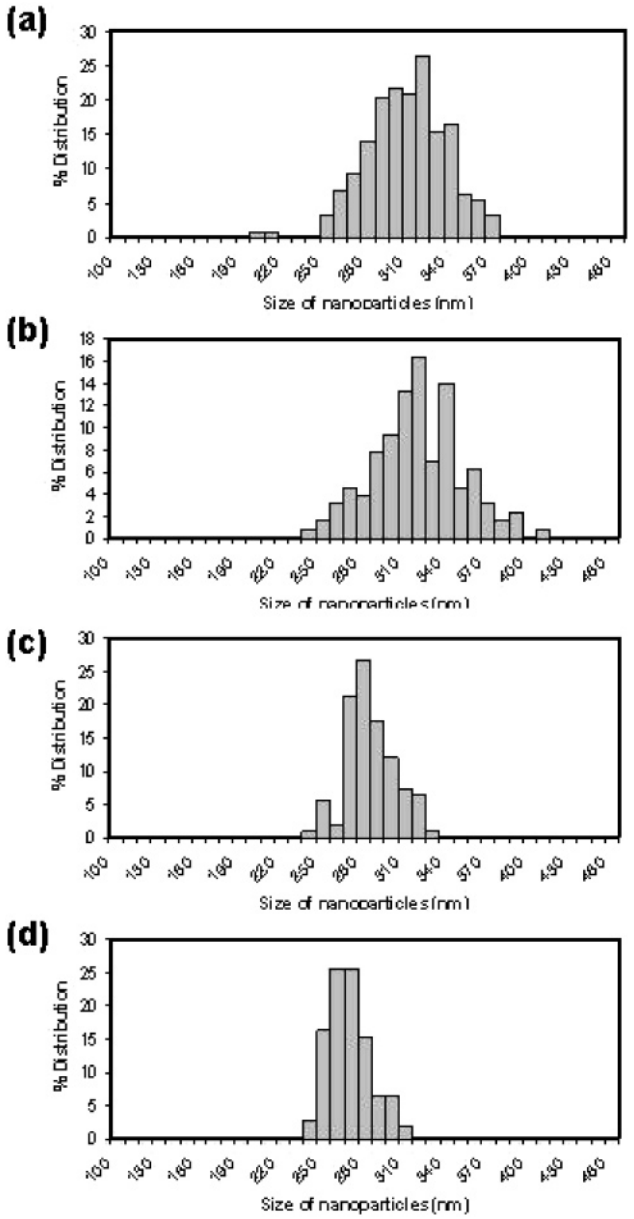

Figure 14. Histograms of size distributions of Au nanoparticles and after annealing at (a) 325, (b) 451, (c) 700, and (d) 930 °C. In this case, the masked substrate was exposed to 12 min of RIE prior to Au deposition and thermal annealing.

min. Figure 16a illustrates the morphology of the Au nanoparticles as-deposited into the etched nanopores in the Si substrate, and Figure 16b shows the annealed and rounded Au nanoparticles in the nanopores. It should be noted that Figure 16 shows images obtained from the same sample before and after annealing, but they do not correspond to an identical area of the sample. During the RIE treatment of a double-layered mask, the top layer of nanospheres is etched in a direction perpendicular to the sample.[24] Thus each nanosphere from the top layer shrinks uniformly. The bottom layer is also etched but is partially shielded by the top. Since they are shielded, bottom layer nanospheres do not change significantly. As a result, the shape of the deposited nanoparticle is expected to change from a hexagonal shape to a quasi-triangular shape with the apex still partially blocked by the upper shrunken nanospheres. After the RIE process, the sample was then transferred to the electron beam evaporation system for the coating of Au film. Bear in mind that the top layer of shrunken nanospheres is no longer packed and thus it is likely that the some of the shrunken

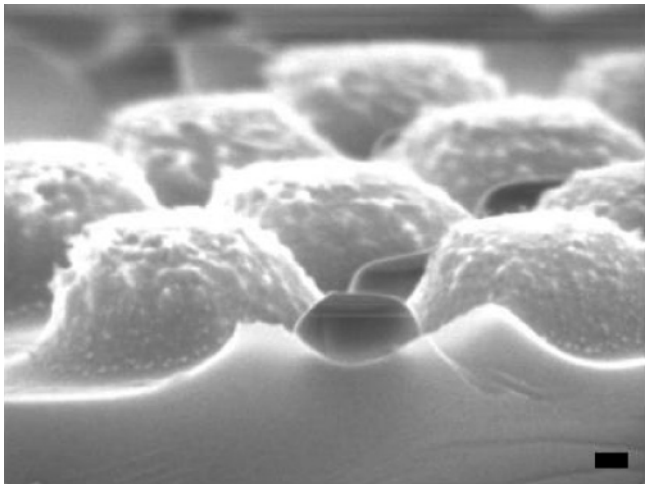

Figure 15. Oblique view SEM image of annealed Au nanoparticle array on etched substrate. Scale bar = 100 nm.

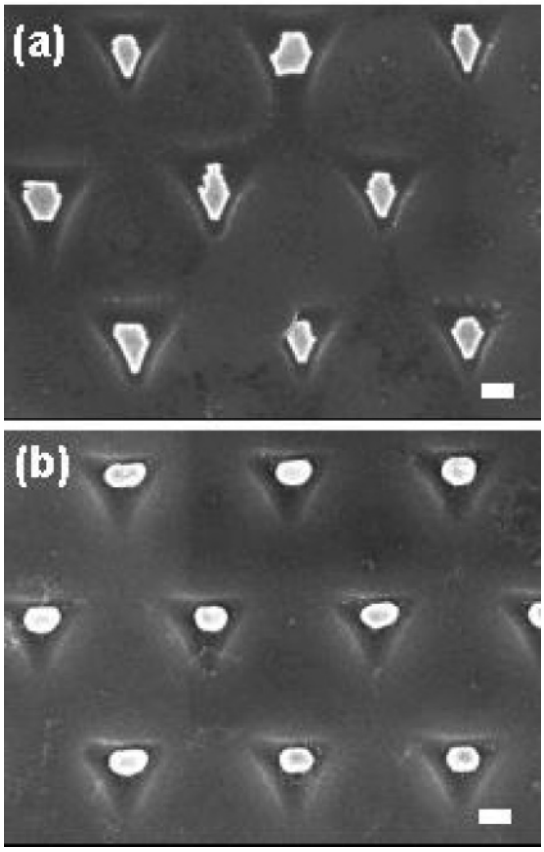

Figure 16. SEM images of (a) Au nanoparticles as-deposited onto region of the etched substrate previously covered with double layer of nanospheres. (b) After thermal annealing at 350 °C, the rounded nanoparticles are caged in the etched pockets. Scale bars = 200 nm.

nanospheres are displaced slightly or toppled during the sample handling and mounting. As a result, instead of the expected quasi-triangular shape, the apex of the deposited Au nanoparticles becomes further truncated as shown in Figure 16a.

It is interesting to note that, with NSL and RIE, one could also create two Au triangular nanodisks that were separated by a very small gap. Figure 17 shows an SEM image of an example of two Au nanodisks separated by a gap of about 8 nm. Such a configuration of Au nanodisks could be potentially useful as electrodes for the assembly of molecules where the molecules can bridge the two electrodes.

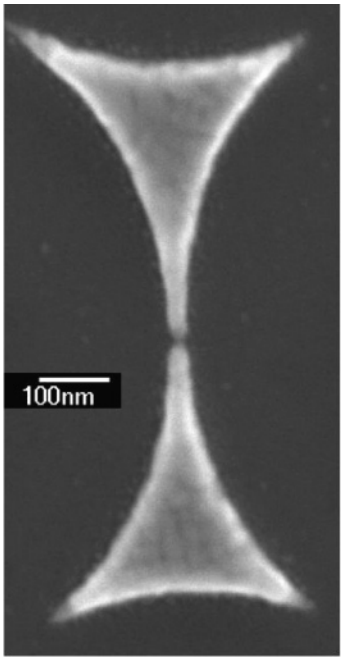

Figure 17. SEM image of two Au nanodisks separated by a nanoscale gap of about 8 nm.

Conclusion

In conclusion, we have further developed two variants of the NSL technique that facilitate more control over the size and shape of the periodic array of Au nanoparticles. In addition, the Au nanoparticles could be confined in the nanopores created on the Si substrate. One potential advantage of having the Au nanoparticles confined in the nanopores is that the Au nanoparticles can serve as a catalyst for growth of other materials (such as such as ZnO nanowires) and the periodic arrangement of the Au nanoparticles would not be disrupted during the synthesis process. Future experiments include extending the techniques to other materials and different types of substrates.

Acknowledgment. C.H.S. acknowledges the support of the National University of Singapore (NUS) Academic Research Fund and the NUS Nanoscience and Nanotechnology Initiative.

References and Notes

(1) Storhoff, J. J.; Elghanian, R.; Micuc, R. C.; Mirkin, C. A.; Letsinger, R. L. *J. Am. Chem. Soc.* **1998**, *120*, 1959−1964.
(2) Mucic, R. C.; Storhoff, J. J.; Letsinger, R. L.; Mirkin, C. A. *Nature* **1996**, *382*, 607.
(3) Haes, A. J.; Hall, W. P.; Chang, L.; Klein, W. L.; Van Duyne, R. P. *Nano Lett.* **2004**, *4*, 1029−1034.
(4) Yonzon, C. R.; Jeoung, E.; Zou, S.; Schatz, G. C.; Mrksich, M.; Van Duyne, R. P. *J. Am. Chem. Soc.* **2004**, *126*, 12669−12676.
(5) Haes, A. J.; Chang, L.; Klein, W. L.; Van Duyne, R. P. *J. Am. Chem. Soc.* **2005**, *127*, 2264−2271.
(6) Weissman, J. M.; Sunkara, H. B.; Tse, A. S.; Asher, S. A. *Science* **1996**, *274*, 959−963.
(7) Asher, S.; Chang, S.-Y.; Tse, A.; Liu, L.; Pan, G.; Wu, Z.; Li, P. *Mater. Res. Soc. Symp. Proc.* **1995**, *374*, 305−310.
(8) Kobayashi, N.; Egami, C.; Kawata, Y.; Fujimura, H.; Sugihara, O. *Jpn. J. Appl. Phys., Part 1* **2002**, *41*, 1907−1908.
(9) Hakanson, U.; Persson, J.; Persson, F.; Svensson, H.; Montelius, L.; Johansson, M. K. J. *Nanotechnology* **2003**, *14*, 675−679.
(10) Chou, S. Y.; Krauss, P. R.; Zhang, W.; Guo, L.; Zhuang, L. *J. Vac. Sci. Technol., B* **1997**, *15*, 2897−2904.
(11) Zhang, H.; Loh, K. P.; Chen, W.; Tan, C. K.; Koh, Y. W.; Sow, C. H.; Lim, C. W. *Diamond Relat. Mater.* **2004**, *13*, 1116−1119.
(12) Banerjee, D.; Rybczynski, J.; Huang, J. Y.; Wang, D. Z.; Kempa, K.; Ren, Z. F. *Appl. Phys. A* **2005**, *80*, 749−752.
(13) Park, K. H.; Lee, S.; Koh, K. H.; Lacerda, R.; Teo, K. B. K.; Milne, W. I. *J. Appl. Phys.* **2005**, *97*, 024311−024314.
(14) Huang, W.; Qian, W.; El-Sayed, M. A. *Nano Lett.* **2004**, *4*, 1741−1747.
(15) Deckman, H. W.; Dunsmuir, J. H. *Appl. Phys. Lett.* **1982**, *41*, 377−379.
(16) Hulteen, J. C.; Van Duyne, R. P. *J. Vac. Sci. Technol., A* **1995**, *13*, 1553−1558.
(17) Haynes, C. L.; Van Duyne, R. P. *J. Phys. Chem. B* **2001**, *105*, 5599−5611.
(18) Jensen, T. R.; Duval, M. L., Kelly, K. L.; Lazarides, A. A.; Schatz, G. C.; Van Duyne, R. P. *J. Phys. Chem. B* **1999**, *103*, 9846−9853.
(19) Li, N.; Zinke-Allmang, M. *Jpn. J. Appl. Phys., Part 1* **2002**, *41*, 4626−4629.
(20) Rybczynski, J.; Ebels, U.; Giersig, M. *Colloids Surf., A* **2003**, *219*, 1−6.
(21) Haginoya, C.; Ishibashi, M.; Koike, K. *Appl. Phys. Lett.* **1997**, *71*, 2934−2936.
(22) Fujimura, T.; Tamura, T.; Itoh, T.; Haginoya, C.; Komori, Y.; Koda, T. *Appl. Phys. Lett.* **2001**, *78*, 1478−1480.
(23) Choi, D.; Yu, H. K.; Jang, S. G.; Yang, S. *J. Am. Chem. Soc.* **2004**, *126*, 7019−7025.
(24) Tan, B. J. Y.; Sow, C. H.; Lim, K. Y.; Cheong, F. C.; Chong, G. L.; Wee, A. T. S.; Ong, C. K. *J. Phys. Chem. B* **2004**, *108*, 18575−18579.
(25) Murray, W. A.; Astilean, S.; Barnes, W. L. *Phys. Rev. B* **2004**, *69*, 165407−165413.
(26) Whitney, A. V.; Myers, B. D.; Van Duyne, R. P. *Nano Lett.* **2004**, *4*, 1507−1511.
(27) Nanda, K. K.; Sahu, S. N.; Behera, S. N. *Phys. Rev. A* **2002**, *66*, 13208−13215.
(28) Wang, Z. L.; Petroski, J. M.; Green, T. C.; El-Sayed, M. A. *J. Phys. Chem. B* **1998**, *102*, 6145−6151.
(29) Hulteen, J. C.; Treichel, D. A.; Smith, M. T.; Duval, M. L.; Jensen, T. R.; Van Duyne, R. P. *J. Phys. Chem. B* **1999**, *103*, 3854−3863.
(30) Julies, B. A.; Adams, D.; Mayer, J. W. *Thin Solid Films* **2004**, 469−470, 282−289
(31) Chang, J. F.; Young, T. F.; Yang, Y. L.; Ueng, H. Y.; Chang, T. C. *Mater. Chem. Phys.* **2004**, *83*, 199−203.
(32) Haynes, C. L.; McFarland, A. D.; Zhao, L. L.; Van Duyne, R. P.; Schatz, G. C.; Gunnarsson, L.; Prikulis, J.; Kasemo, B.; Kall, M. *J. Phys. Chem. B* **2003**, *107*, 7337−7342.
(33) Yin, Y.; Lu, Y.; Gates, B.; Xia, Y. N. *J. Am. Chem. Soc.* **2001**, *123*, 8718−8729.
(34) Hoogenboom, J. P.; Retif, C.; de Bres, E.; van de Boer, M.; van Langen-Suurling, A. K.; Romijn, J.; van Blaaderen, A. *Nano Lett.* **2004**, *4*, 205−208.
(35) Velikov, K. P.; Christova, C. G.; Dullens, R. P. A.; van Blaaderen, A. *Science* **2002**, *296*, 106−109.
(36) Yang, S. M.; Ozin, G. A. *Chem. Commun.* **2000**, *24*, 2507−2508.
(37) Jo, S. H.; Lao, J. Y.; Ren, Z. F.; Farrer, R. A.; Baldacchini, T.; Fourkas, J. T. *Appl. Phys. Lett.* **2003**, *83*, 4821−4823.
(38) Park, J.; Choi, H. H.; Siebein, K.; Singh, R. K. *J. Cryst. Growth* **2003**, *258*, 342−348.